

# Summary of the SPHN activities in the PHENIX experiment at RHIC: measuring the $J/\psi$ production in relativistic $p + p$ , $d + A$ and $A + A$ collisions at a center of mass energy $\sqrt{s_{\text{NN}}} = 200$ GeV

Alberto Baldisseri, Hervé Borel, Javier Castillo, Jean-Luc Charvet, Claudio Geuna,  
Hugo Pereira Da Costa, Andry Rakotozafindrabe, Hongyan Yang

March 26, 2012

## 1 Introduction

The PHENIX experiment [1] is one of the two large experiments located on the Relativistic Heavy Ion Collider (RHIC) at the Brookhaven National Laboratory (BNL), in Long Island, United States. It aims to study the properties of the nuclear matter under conditions of high pressure and high temperature, such as the conditions achieved during relativistic heavy ion collisions and notably to evidence the formation of a Quark Gluon Plasma (QGP), a state of the nuclear matter in which quarks and gluons are no longer bound into nucleons but can on the contrary travel quasi-freely on distances that are larger than the typical nucleon size.

A variety of observables can be measured in order to achieve these goals, and notably the production of the  $J/\psi$  resonance, the first bound state of a  $c$  and  $\bar{c}$  quark pair that is stable for the strong interaction. The heavy mass of the charm quark ( $m_c = 1.27_{-0.11}^{+0.7}$  GeV/ $c^2$ ) and consequently of the  $J/\psi$  meson ( $m_{J/\psi} = 3.097$  GeV/ $c^2$ ) implies that it is mainly created in the early stage of a nucleus-nucleus collision, via the hard scattering of two partons (dominantly two gluons, at RHIC energy), thus making it sensitive to the subsequent evolution of the collision.

The production of the  $J/\psi$  meson was originally predicted to be reduced in the presence of a QGP by a color screening mechanism, similar to the Debye screening of electromagnetic charges in QED, that would prevent the primordial  $c\bar{c}$  pairs to form a bound state [2]. Later on, a number of additional effects have been identified that can affect the production of the  $J/\psi$  particle in nucleus-nucleus collisions with respect to its appropriately scaled production in  $p + p$  collisions, thus making it more complicated to interpret the results obtained in  $A + A$  collisions in terms of the formation of a QGP. Some of these effects do not imply the formation of the QGP and are therefore called *cold nuclear matter* effects. They include [3]:

- the modification of the parton distribution functions inside a nucleon depending on whether the nucleon is isolated or within a nucleus;
- the energy lost by the incoming partons (mostly gluons, at RHIC energies) by multiple scattering against other partons in the nucleus before forming a  $c\bar{c}$  pair (and later on a  $J/\psi$ );
- the breakup of the  $J/\psi$  meson or of its pre-resonant  $c\bar{c}$  state by interaction with the surrounding hadrons, formed during the collision.

Other effects beyond the color screening mechanism mentioned above have also been proposed to modify the production of the  $J/\psi$  meson in the presence of a QGP, and notably a possible enhancement of the

$J/\psi$  yield due to the coalescence of uncorrelated  $c\bar{c}$  pairs from the hot medium [4, 5, 6]. However, the applicability of such a mechanism to the energy densities achieved at RHIC is still debated.

Consequently, the following three steps are needed to study the influence of the formation of a QGP on the production of the  $J/\psi$  meson:

- measure the  $J/\psi$  production cross section in  $p + p$  collisions, to serve as a reference;
- measure its cross section in  $p + A$  (or  $d + A$  at RHIC) collisions, for which a QGP is not expected to be formed, in order to quantify the cold nuclear matter effects;
- measure its cross section in  $A + A$  collisions (notably as a function of the collision's impact parameter) to identify modifications beyond the cold nuclear matter effects measured in  $d + A$ , that can then be attributed to the presence of a QGP.

The SPHN joined the PHENIX experiment at the end of the year 2000 together with several groups from the IN2P3, inside the PHENIX-France collaboration. Its original contribution was to finance 25% of the readout electronics of the PHENIX forward rapidity muon spectrometers, dedicated to the measurement of muons at forward rapidity. Until the end of the year 2010, at which time the SPHN has officially left the collaboration to focus on the ALICE experiment [7], on the Large Hadron Collider (LHC), at CERN, our group has been active in the following fields:

- on the hardware side, beside the mandatory shifts that all the scientist participating to the experiment must take during data taking, we have contributed to the maintenance of the muon spectrometers during the shutdown periods of the detector;
- on the software side, we have participated in rewriting the track reconstruction algorithm at forward rapidity in preparation of the first high luminosity Au + Au run at RHIC in 2004 and have remained in charge of the development and maintenance of this algorithm since then. We have also become responsible for all the simulations of the experiment, needed to correct PHENIX measurements from the detector's acceptance and inefficiencies in order to derive physical quantities. Finally we have also implemented the algorithm needed to evaluate and monitor the alignment of the muon spectrometer, based on reconstructed tracks with and without magnetic field.
- on the analysis side, we have played a leading role in all analysis that involve the production of the  $J/\psi$  meson at forward rapidity, and their interpretation in terms of the properties of the nuclear matter created in  $p + p$ ,  $d + A$  and  $A + A$  collisions. As such we have been part of the internal Paper Publication Group of almost all  $J/\psi$  related PHENIX publications, since 2007 [8, 9, 10, 11, 12, 13].

This document is organized as follows:

- sections 2 and 3 briefly describe the PHENIX apparatus, and notably its two forward rapidity muon spectrometers;
- sections 4 to 6 summarize our implication on the PHENIX software;
- sections 7 to 10 focus on the results obtained for the production of the  $J/\psi$  resonance at RHIC and their interpretation in terms of a QGP formation.

## 2 The PHENIX Experiment

Figure 1 shows two schematic views of the PHENIX detector [1]. It consists of two central spectrometers which measure particles produced at mid-rapidity (that is, in the direction perpendicular to the beams

axis),  $|\eta| < 0.35$ , and two muon spectrometers which measure particles produced at forward rapidity,  $1.2 < |\eta| < 2.2$ . The central detectors are constituted of several subsystems listed in figure 1. They provide good particle identification and momentum reconstruction down to  $p_T = 0.2 \text{ GeV}/c$ . They notably measure hadrons, photons and electrons, and have an azimuthal coverage  $\delta\Phi = \pi$ . The muon spectrometers are located behind two frontal absorbers on both sides of the interaction point that stop most of the hadrons produced at forward rapidity during the collision. They measure principally muons down to a momentum  $p = 2 \text{ GeV}/c$  and have full azimuthal coverage.

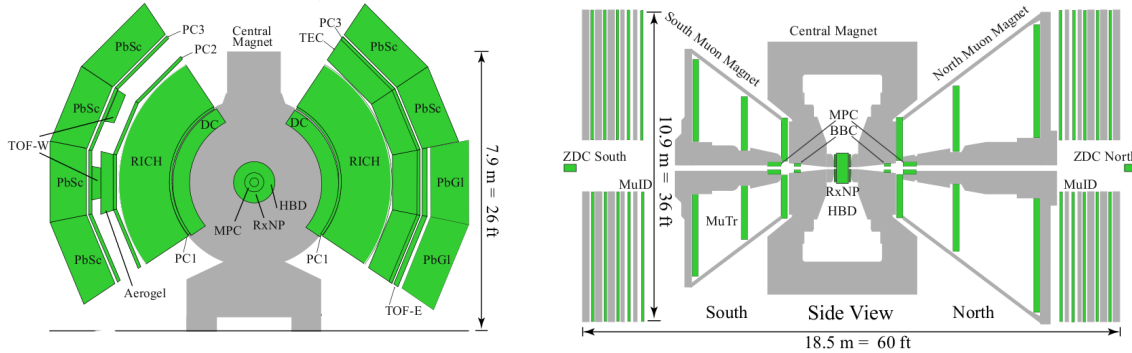


Figure 1: Schematic view of the PHENIX experiment. Left: front view of the central detectors; right: side view of the muon spectrometers.

Additional detectors, namely the Beam Beam Counters (BBC), the Zero Degree Calorimeters (ZDC) and the Reaction Plane detector (RXnP), are used to measure the position of the collision vertex along the beam axis, the collision's centrality and the azimuthal orientation of the collision's *reaction plane*, formed by the beam axis and the vector that joins the center of the two colliding nuclei.

### 3 The PHENIX Forward Rapidity Muon Spectrometers

Each PHENIX muon spectrometer is located behind an iron and copper frontal absorber that stops most of the hadrons produced during the collision and is constituted of two parts: the muon identifier (MuID) and the muon tracker (MuTr).

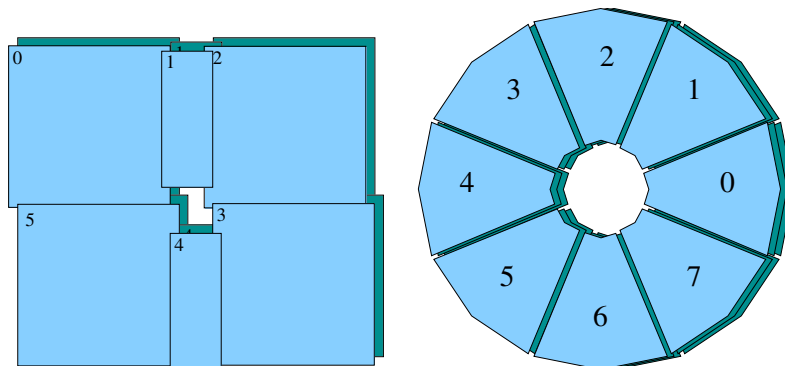


Figure 2: Schematic view of one detection element of the two subsystems that constitute PHENIX muon spectrometers. Left: one muon identifier (MuID) gap; right: one muon tracker (MuTr) station.

The muon identifier consists of five alternating layers of detection elements (so-called gaps) and steel

absorbers. Each gap consists of two layers of horizontal and vertical Iarocci tubes, segmented into six panels, around the beam pipe, as shown in the left panel of figure 2. The use of alternating layers of detection elements and absorber allows one to correlate a given muon’s momentum to its penetration depth in the MuID (the last gap in which this muon is detected): a minimum energy of  $\sim 1.9$  GeV is required for a muon to reach the first gap of the MuID. It must have at least  $\sim 2.7$  GeV to reach the last gap. On the other hand, the probability for a hadron (mostly pions) produced during the collision to reach the last gap of the MuID without being stopped in any of the absorbers described above is about  $2.5 \times 10^{-4}$ .

In total, the MuID has about 1300 Iarocci tubes, grouped two by two, resulting in about 6500 readout channels.

The MuID is used to trigger on muons (as opposed to hadrons) that have enough momentum to penetrate the steel absorber layers. The straight track segments reconstructed in the MuID are also used as a seed to the full track reconstruction in the MuTr, in the data analysis.

The muon tracker consists of three stations of Cathode Strip chambers. The first and second stations have three chambers each and the third station has two chambers. Each station is further divided in height octants, around the beam pipe, as illustrated in the right panel of figure 2, which are in turn divided into two half-octants each. Both cathodes of each octant are segmented into strips of width 0.5cm and with a spacing of 1cm. Every two cathodes has its strips parallel to the half-octant median (and therefore along the radial direction), and are called the non-stereo planes. The other cathodes are called the stereo plane and have strips that form a small angle with respect to the half-octant’s median which range between  $3.75^\circ$  and  $11.75^\circ$ , depending on the plane. The chambers resides in an approximately radial magnetic field, generated by a solenoid magnet that surrounds the beam pipe.

In total, the MuTr has about 45000 strips (and as many readout channels), whose length can reach 3 meters (in the third station). It constitutes the largest subsystem (both in terms of size and numbers of readout channels) of the PHENIX spectrometer.

The MuTr is used to measure the momentum and position of the particles that traverse the frontal absorber. These track parameters are then extrapolated (backward) towards the interaction point in order to determine the particle’s properties at the collision point.

## 4 Track Reconstruction in the Muon Spectrometers

The track reconstruction algorithm aims at determining the combinations of hits in the MuID and in the MuTr that correspond to the passing of a single particle through the detector, and measuring the position and momentum of this particle, using a fit to the hit positions.

The algorithm starts by finding straight segments of tracks in the MuID (for which there is no magnetic field that would bend the trajectory of the particles). Vertical and horizontal planes are handled independently and segments found in a given MuID panel for both directions are combined two by two to form 3-dimensional track segments. Only segments that approximately points to the interaction point are kept, in order to reject secondary particles, cosmic rays, or particles coming from the interaction of the beam with either the beam pipe or the beam gas. These segments are extrapolated to the third station of the MuTr, and hits found there in the vicinity of the extrapolated segment are added to the track. The same procedure is repeated for the MuTr second and first station. At each step, tracks for which an insufficient number of matching hits is found are rejected. On the contrary, when several hits are found that match a given extrapolated segment, the track is *duplicated* and the resulting two segments are then handled independently. An additional difficulty for finding tracks in the MuTr comes from the fact that the magnetic field cannot be neglected, and that the resulting bending of the particle’s trajectory must be accounted for when extrapolating from one station to the other. This requires that the particle’s momentum is estimated at each step, which is achieved by using a simple parametrisation of the trajectory’s bending inside the

magnetic field as a function of the particle’s momentum. This so-called *bend-plane* parametrization provides a less precise estimate of the particle’s momentum than the Kalman filter performed in the next step but is much faster and therefore better suited to finding the right combinations of hits that correspond to the same particle.

Once combinations of hits associated to a single particle are found, a full fit of the corresponding positions is performed in order to determine the particle’s momentum in the first station of the MuTr. The fit is only performed on the combinations that satisfy a number of quality selection criteria based notably on the number of hits found in each station. It utilizes a Kalman filter technique [14] whose current version has been implemented by the SPHN group and is faster (and at least as precise) as a standard least-square minimization. This technique allows one to properly account for the magnetic field in the MuTr and the propagation of errors from one station to the other, including notably, the error increase due to the particle’s multiple scattering in the detector’s material. As a by-product, the Kalman filter also provides the track position and momentum in each of the MuTr and MuID detector planes (with proper accounting for the particle energy loss through matter), which can then be used to further reject tracks of poor quality.

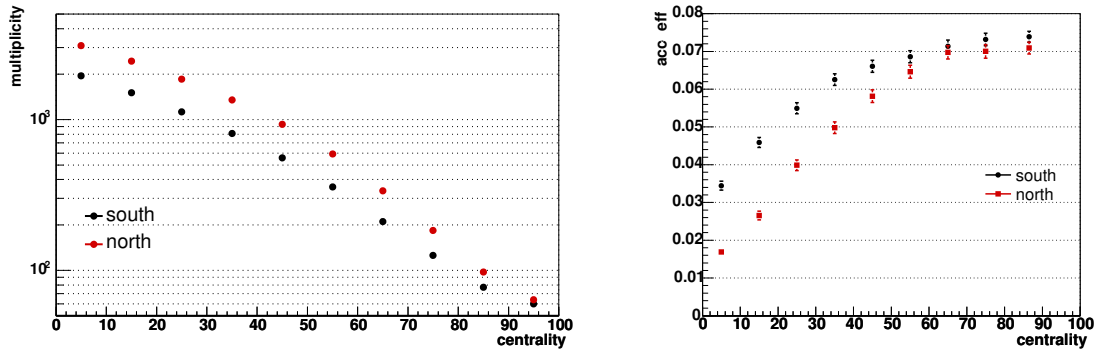


Figure 3: Left: total hit multiplicity in the muon spectrometers as a function of the collision’s centrality in Au + Au collisions; right: acceptance and efficiency corrections for the production of the  $J/\psi$  resonance at forward rapidity ( $1.2 < |y| < 2.2$ ) as a function of the centrality.

For  $p + p$  collisions and peripheral A + A collisions (large values of the impact parameter  $b$ , the distance between the centers of the two colliding nuclei), the track finding algorithm described above has an efficiency larger than 80 % (with most of the inefficiencies coming from the strict track quality cuts needed to reject background tracks and fortuitous combinations of hits). However, when the hit multiplicity increases in the detector for more central collisions (smaller values of the impact parameter), this efficiency drops significantly. This is illustrated in the right panel of figure 3, which represents the acceptance and efficiency corrections for  $J/\psi$  produced in Au + Au collisions as a function of the collision centrality. These corrections, estimated by means of simulations, are needed to calculate the number of produced  $J/\psi$  in a given rapidity range (here  $1.2 < |y| < 2.2$ ) from the number of  $J/\psi$  measured in the detector. There are several contributions to the acceptance and efficiency corrections:

- the detector geometrical acceptance: a significant fraction of the  $J/\psi$  decay muons end up outside of the detector angular acceptance or inside its dead areas and cannot be reconstructed because of not leaving hits in the detectors;
- the detector’s intrinsic inefficiencies, and its dead areas due to time-dependant hardware failures (tripped high voltage, disabled front-end electronic channels, etc.);
- track reconstruction and quality cuts inefficiencies, corresponding to muons which, despite the fact that they do leave hits in the detectors, are not reconstructed properly or even simply discarded.

The first two contributions are hardware related and do not depend on the collision’s centrality. In figure 3,

they amount to a correction of about 9 to 10 %. The remaining effect (from 10 % down to  $\sim 7$  % for peripheral collisions) and the visible centrality dependence of the acceptance and efficiency corrections are attributed to the third, software related, contribution, and could in principle be improved with a more efficient reconstruction algorithm. The significant decrease of the efficiency, by about a factor 4 between most central and most peripheral collisions with increasing hit multiplicity in the detector is attributed to the presence of an increasing fraction of overlapping clusters in the detectors, corresponding to strips that are hit by two different particles in the same event, and which are not fitted properly, resulting in offsets of several millimeters between the true particle position and the measured position. Such offsets result in either poorly reconstructed tracks with large chi-square, or the track not being reconstructed at all. So far it has not been possible to successfully overcome this effect while keeping the contamination of fake tracks (fortuitous combination of hits) to a small enough level.

## 5 Detector alignment

The precise measurement the particle's momentum requires that one knows accurately the position of the detectors relative one to the other and relative to the magnetic field. During the construction of the spectrometer a survey of the detector's position is performed and this is used later on in both the simulations and the track reconstruction. However, this description is usually not precise enough, and becomes less accurate over time, as detectors are moved, notably for repairs. As a consequence, an offline alignment procedure is used periodically, based on the quality of the reconstructed tracks, that calculates corrections to the initial survey so that the expected position of the detectors match their true position better.

The calculation of these alignment corrections can be achieved by assuming that the position of a given subset of the detectors is known perfectly, using these detectors as reference to calculate the trajectory of the particles and comparing these trajectories to the hits found in the other detectors, not used in the track reconstruction. One forms so called *residual* distributions by comparing the expected particle's hit position in the detector with the corresponding measured hit position and manually adjusting the detector's position so that this distribution becomes centered on zero. One then changes the set of reference detectors for the second and subsequent iterations until all residual's distributions are well centered. Such a method is time consuming since the full track reconstruction must be performed at each iteration; it uses only a fraction of the information (the mean value of the residual distributions) and it is not guaranteed to converge to a set of corrections that is independent of the initial set of reference detectors.

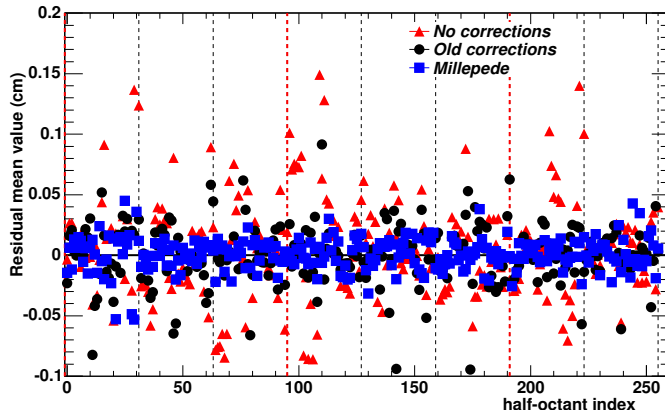


Figure 4: Mean value of the residual distribution in each half-octant of the MuTr as a function of the detector index for three sets of alignment corrections.

An alternative approach has been developed and implemented for PHENIX and for other physics exper-

iment that takes advantage of the detector’s redundancy to simultaneously minimize the chi-square of many reconstructed tracks as a function of both the track parameters and the detector’s position (that is independent from the tracks passing through it) [15]. In principle, such a minimization requires only one iteration and uses all the available information, notably because all the detectors are used simultaneously to reconstruct the tracks that enter the chi-square. A limited set of detectors still needs to be fixed that is smaller than for the manual, iterative method described above, in order to prevent global transformations of the whole spectrometer that would leave the track chi-square unchanged.

Figure 4 illustrates the performances of this so-called *global* method, compared to the initial detector survey, and the alignment corrections previously obtained with the iterative method. Shown are the mean value of the residual distributions in each half-octant of the muon tracker as a function of the half-octant index, once all detectors are included in the tracking. Residuals obtained with the global method are better centered around zero than with any other set of alignment corrections. However, there remains significant deviations from zero (of order several hundred micrometers) that are attributed to the finite number of tracks used for the minimization and to the fact that not all possible displacements of the detectors have been accounted for in the chi-square.

## 6 Simulations

Simulations are required for all physics analysis to

- quantify and understand the detector and analysis software performances;
- study the detector response to a given physics signal and estimate the relevant background sources;
- correct the measured data by the detector acceptance and both hardware and software inefficiencies in order to obtain detector independent quantities such as invariant production yields or cross sections.

In PHENIX, the full simulation chain is composed of three steps:

- generate an event by event particle sample at the collision point, possibly enriched with a specific physics signal, such as the production of a  $J/\psi$  and its decay in two leptons. This is achieved using event generators such as PYTHIA [16], HERWIG [17], HIJING [18], or home made *fast* event generator;
- propagate the generated set of primary particles through the detector, possibly generating secondary particles in the process, while properly accounting for the magnetic fields and the effect of detector materials in terms of multiple scattering and energy loss and derive the corresponding set of *ideal* particle hits in the detectors. This is achieved using a GEANT3 [19] simulation of the PHENIX detectors;
- apply corrections to the generated ideal hits in order to account for the detector’s response to particles passing through it. This includes notably the accounting for time dependant dead areas, the applications of detector calibrations and thresholds and the possible addition of electronic noise. The resulting *realistic* event-by-event set of hits should then be identical to what comes out of the real data taking, and can be reconstructed using the same software and analysis cuts as real data.

This last step is crucial to the measurement of absolute physics quantities (such as production cross sections) with the PHENIX detector. It requires a precise book-keeping of the detector performances during data taking and a precise modelling of these performances in the simulations. The accuracy of this modelling is controlled by comparing a set of low level observables that can be measured both in real data and simulations, such as the azimuthal distribution of the reconstructed tracks, as illustrated in figure 5 [20]. An overall good agreement is achieved between the real data and the simulated distributions.

Regions of the detector where significant differences are observed must be excluded from the analysis. Remaining residual differences must be accounted for in the systematic uncertainty associated to the measurement of physics quantities.

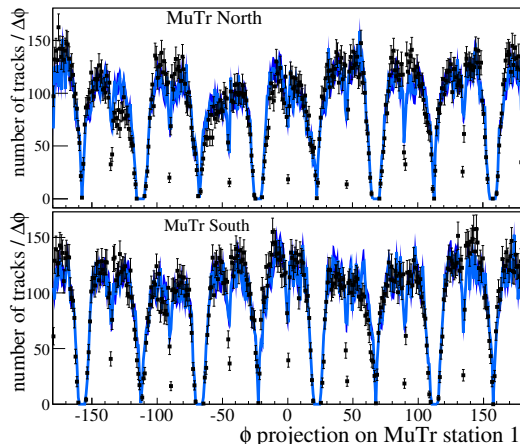


Figure 5: Comparison of the azimuthal distributions of the reconstructed tracks in a real data sample (markers) and in simulations (solid lines) in the muon spectrometers.

Simulations are also used to test the addition of new detectors to the existing spectrometer, and measure their impact on its ability to perform new physics measurements. Three such detectors have been studied in the period during which our group have been in charge of the PHENIX simulations:

- the Hadron Blind Detector, located in the center of the PHENIX spectrometer around the interaction point, which is a Cerenkov detector dedicated to the detection of electrons produced during a collision and transparent to hadrons; this detector have been operated intermittently between 2007 and 2010;
- the barrel and forward silicon vertex detectors (VTX and FVTX), two thin high granularity and high resolution vertex detectors that surround the interaction point (in replacement of the HBD described above) and should provide precise secondary vertex detection and track reconstruction near the collision point at both mid- and forward rapidity. The barrel detector has been installed and operated for the first time in 2011. The forward detector will be operated starting from 2012;
- the Nose Cone Calorimeter, a calorimeter located at forward rapidity in replacement of a fraction of the muon spectrometers' frontal absorber and dedicated to the forward rapidity physics in  $p + p$  and possibly  $d + Au$  collisions. The construction and installation of this detector is still debated inside the PHENIX collaboration.

## 7 Di-leptons Invariant Mass Distributions

$J/\psi$  particles are measured in the PHENIX central spectrometer using their decay in two electrons and in the muon spectrometers using their decay in two muons. The number of  $J/\psi$  mesons in a given rapidity and  $p_T$  bin is estimated using the invariant mass distribution of the unlike-sign pairs of leptons found in the same event. This distribution has three contributions:

- the combinatorial background, constituted by pairs of uncorrelated leptons;
- the physical background, constituted by pairs of leptons which are correlated by an underlying physics process but do not form a resonance peak. In the mass range of interest (2 to 6  $\text{GeV}/c^2$ ), these processes are the Drell-Yan production and D meson pair production, followed by a semi-leptonic decay of both mesons;

- the resonance signals, from the  $J/\psi$  ( $M = 3.1 \text{ GeV}/c^2$ ) and  $\psi'$  ( $M = 3.1 \text{ GeV}/c^2$ ) mesons.

The contribution from the combinatorial background is estimated using either the invariant mass distribution of the same-event like-sign lepton pairs or an event mixing technique that consists of forming the invariant mass distribution of pairs of leptons that do not belong to the same event, normalized to the same-event distributions using the like-sign lepton pairs. The physical background contribution is estimated using either empirical or simulation driven fits to the data, outside of the mass range that correspond to the resonances. The  $J/\psi$  signal is then evaluated using either simple counting of the number of hits above the previous two contributions, or with a dedicated fit of the resonance line-shape, performed simultaneously to the physical background fit.

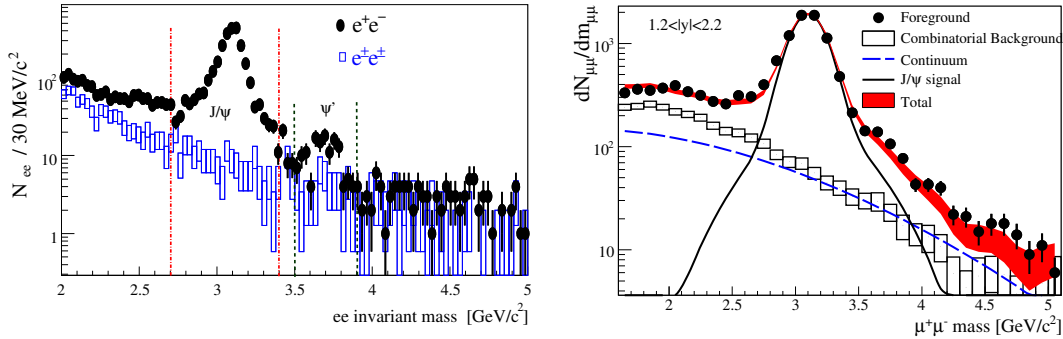


Figure 6: Di-lepton invariant mass distributions in  $\sqrt{s} = 200 \text{ GeV}$   $p + p$  collisions, measured at mid-rapidity in the di-electron channel (left panel) and at forward rapidity in the di-muon channel (right panel).

Figure 6 shows two example invariant mass distributions obtained at mid and forward rapidities in  $p + p$  collisions, together with the three contributions described above [20].

## 8 $J/\psi$ Production in $p + p$ Collisions

To study the  $J/\psi$  production in  $p + p$  collisions, two quantities have been measured as a function of the  $J/\psi$  rapidity and transverse momentum: the  $J/\psi$  invariant yield and the  $J/\psi$  production cross section. The  $J/\psi$  invariant yield in a given  $y$  and  $p_T$  bin is written:

$$\frac{B_{ll}}{2\pi p_T} \frac{d^2 N_{J/\psi}}{dp_T dy} = \frac{1}{2\pi p_T \Delta p_T \Delta y} \frac{N_{J/\psi}}{N_{\text{BBC}}} \frac{\varepsilon_{\text{BBC}}^{\text{MB}}}{\varepsilon_{\text{BBC}}^{J/\psi}} \quad (1)$$

where  $B_{ll}$  is the branching ratio of  $J/\psi$  decay in two leptons (muons at forward rapidity and electrons at mid-rapidity);  $N_{J/\psi}$  is the number of  $J/\psi$  mesons measured in the  $y$  and  $p_T$  bin being considered;  $N_{\text{BBC}}$  the number of triggered events (here using the BBC detectors) for the analysed data sample;  $A\varepsilon$  the acceptance and efficiency correction for measuring  $J/\psi$ s in the detector;  $\varepsilon_{\text{BBC}}^{\text{MB}}$  the trigger efficiency for minimum bias inelastic  $p + p$  collisions and  $\varepsilon_{\text{BBC}}^{J/\psi}$  the trigger efficiency for inelastic  $p + p$  collisions that contain a  $J/\psi$  in the final state.

The  $J/\psi$  production cross section is obtained by multiplying the  $J/\psi$  invariant yield by the total  $p + p$  inelastic cross section  $\sigma_{p+p}^{\text{inel}}$ :

$$\frac{B_{ll}}{2\pi p_T} \frac{d^2 \sigma_{p+p}^{J/\psi}}{dp_T dy} = \frac{B_{ll}}{2\pi p_T} \frac{d^2 N_{J/\psi}}{dp_T dy} \sigma_{p+p}^{\text{inel}} \quad (2)$$

Latest results measured by PHENIX [20] are shown in figure 7 and compared to several theoretical calculations which correspond to different  $J/\psi$  production mechanisms and different parton distribution functions

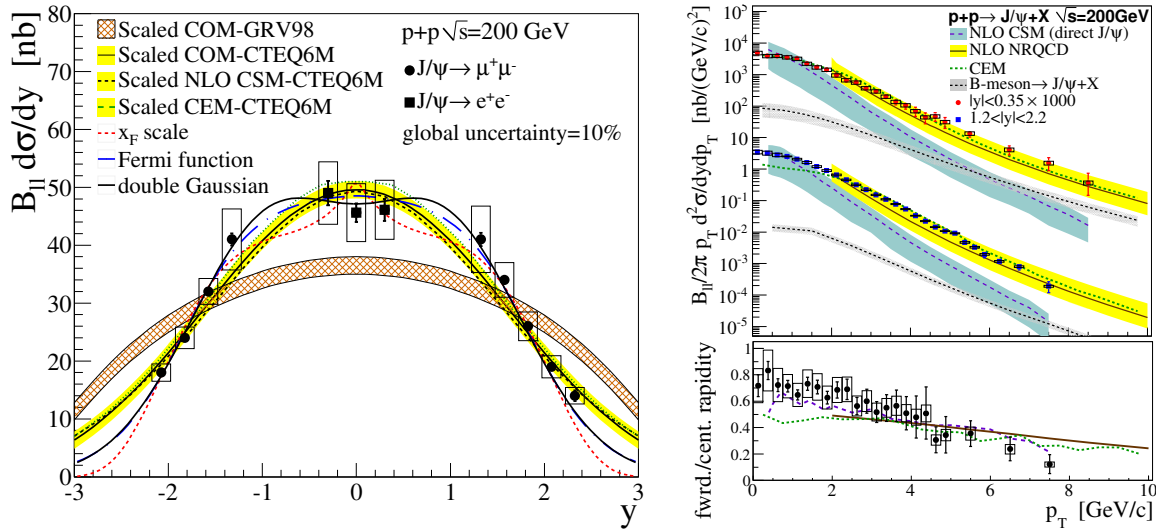


Figure 7: inclusive  $J/\psi$  production cross section in 200 GeV  $p + p$  collisions and comparison to models, left: as a function of the  $J/\psi$  rapidity; right: as a function of the  $J/\psi$  transverse momentum. Also shown in the right panel is the ratio between the forward and mid-rapidity production cross sections.

in the nucleon. There are mainly three models available to describe the formation of a color neutral  $J/\psi$  meson out of a colored  $c\bar{c}$  pair resulting from a hard parton interaction: the Color Evaporation Model (CEM) [21, 22]; the Color Singlet Model (CSM) [23] and the Color Octet Model (COM, or NRQCD, for Non Relativistic Quantum Chromo-Dynamics) [24]. These models differ mainly in how the additional gluons needed to neutralize the  $c\bar{c}$  pair are handled in the calculation. Some of the calculations shown in the left panel of figure 7 are unable to reproduce the measured rapidity dependence of the  $J/\psi$  cross section and can therefore be excluded, this even though they are arbitrarily normalized to the data.

Note that the  $J/\psi$  measurements presented in this section and the following are inclusive and contain contributions from both direct  $J/\psi$  production and feed-down from higher mass quarkonia ( $\psi'$  and  $\chi_c$ ) as well as B hadron decays.

The rapidity distribution of the  $J/\psi$  production cross section is used to calculate a total inclusive  $J/\psi$  production cross section (over the full phase space) in 200 GeV  $p + p$  collisions [20]:

$$B_{II}\sigma_{p+p}^{J/\psi} = 178 \pm 3.0(\text{stat}) \pm 53(\text{syst}) \quad (3)$$

## 9 $J/\psi$ Production in $d + \text{Au}$ Collisions

The  $J/\psi$  invariant yields and production cross sections have been measured in  $d + \text{Au}$  collisions, and compared to the values obtained in  $p + p$  collisions in order to evaluate possible modifications of the  $J/\psi$  production in nucleus-nucleus collisions in absence of a quark gluon plasma. To perform this comparison, the so-called nuclear modification factor  $R_{AA}$  (or here  $R_{d+\text{Au}}$ ) is used :

$$R_{d+\text{Au}} = \frac{dN_{d+\text{Au}}^{J/\psi}/dy}{\langle N_{\text{coll}} \rangle dN_{p+p}^{J/\psi}/dy} \quad (4)$$

where the numerator is the  $J/\psi$  invariant yield measured in  $d + \text{Au}$  collisions (here as a function of rapidity and integrated over  $p_T$ ) and the denominator is the  $J/\psi$  invariant yield measured in  $p + p$  collisions, scaled by  $\langle N_{\text{coll}} \rangle$ , the average number of nucleon-nucleon collisions corresponding to one  $d + \text{Au}$  collision in a given centrality bin.  $N_{\text{coll}}$  is estimated for a given impact parameter using a simple geometrical description of the two nuclei, also known as Glauber model [25].

Measuring a nuclear modification factor  $R_{d+Au}$  equal to unity implies that

- a  $d + Au$  collision can be described as a succession of independent (that is: incoherent) nucleon-nucleon collisions, for the process of interest (here the production of a  $J/\psi$  meson);
- $J/\psi$  produced in one of these independent nucleon-nucleon collisions are not affected by the presence of the surrounding nucleons, or the products of their collisions.

Deviations from unity require that one or several of the above properties is not fulfilled and are indicative of nuclear effects.

Another ratio of interest is the central to peripheral ratio  $R_{CP}$  obtained by dividing the  $J/\psi$  production yields in central  $d + Au$  (or  $A + A$ ) collisions to the yield measured in peripheral collisions, properly normalized by the corresponding values of  $N_{coll}$ :

$$R_{CP} = \frac{dN_{central}^{J/\psi}/dy}{dN_{peripheral}^{J/\psi}/dy} \cdot \frac{\langle N_{coll} \rangle_{peripheral}}{\langle N_{coll} \rangle_{central}} \quad (5)$$

The advantage of using  $R_{CP}$  instead of  $R_{AA}$  is that a  $p + p$  reference is not required and that many experimental systematic uncertainties cancel in the ratio. However, the interpretation of measured values for  $R_{CP}$  is usually more difficult since peripheral  $d + Au$  collisions, which serve as a reference in that case, are less understood than  $p + p$  collisions, as used for the denominator of  $R_{d+Au}$ .

Figure 8 shows the  $J/\psi$  nuclear modification factor  $R_{d+Au}$  for peripheral collisions (top), central collisions (middle), and the central to peripheral ratio  $R_{CP}$  (bottom) as a function of the  $J/\psi$  rapidity [12].

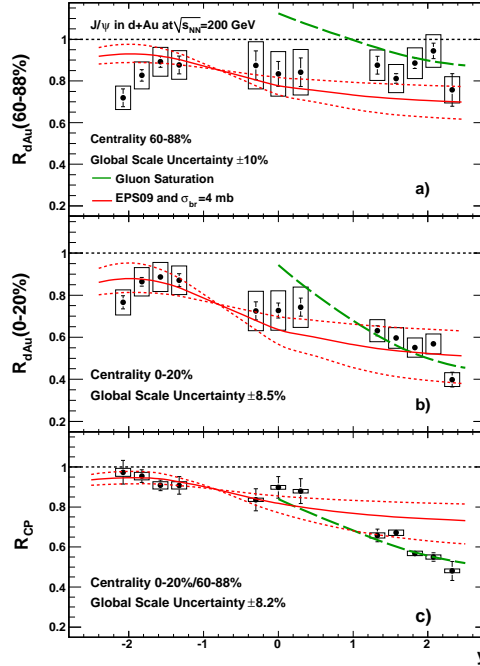


Figure 8: Top:  $J/\psi$  nuclear modification factor  $R_{d+Au}$  as a function of the  $J/\psi$  rapidity for peripheral  $d + Au$  collisions (60-88%); middle:  $J/\psi$   $R_{d+Au}$  for central collisions (0-20%); bottom:  $J/\psi$  central to peripheral ratio  $R_{CP}$ .

Negative rapidity corresponds to the gold-going side of the collisions. The  $J/\psi$  mesons produced in this regime originate dominantly from a large  $x$  gluon from the gold nucleus (with  $x$  being the fraction of the

nucleon longitudinal momentum carried by the gluon inside the gold nucleus, that collides with a gluon from the deuteron nucleus to form a  $c\bar{c}$  pair). Already for peripheral collisions, a suppression of the  $J/\psi$  yield is observed with respect to scaled expectations from  $p + p$  collisions. It is largely independent from the centrality, and has little dependence on rapidity.

On the contrary, positive rapidity corresponds to the deuteron-going side of the collisions. The  $J/\psi$  mesons produced in this regime originate dominantly from a small  $x$  gluon from the gold nucleus. A larger suppression of the  $J/\psi$  yield is observed, which increases for more central collisions, and for more forward (larger values of  $y$ )  $J/\psi$ s.

Two types of calculations are compared to the data in figure 8. The first calculation follows the prescriptions outlined in [26] and includes the following two effects:

- the modification of the nucleon parton distribution functions (which describe the parton density for a given longitudinal momentum fraction  $x$ ) when the nucleon is inside a nucleus with respect to when it is isolated. These modifications are parametrised based on fits notably to Deep Inelastic Scattering experiments, combined to a given  $J/\psi$  production mechanism (here the color evaporation model) to calculate  $J/\psi$  yield ratios. The parametrisation shown here is called EPS09 [27] and includes uncertainties associated to the functional forms used for the fits as well as the experimental uncertainties;
- the nuclear breakup of the  $J/\psi$  (or its pre-resonant  $c\bar{c}$  state), parametrized with a rapidity independent break-up cross section.

This approach is unable to properly describe simultaneously the peripheral and the central data, as is best illustrated by comparing the predicted  $R_{CP}$  to the measured one (bottom panel of figure 8).

The second approach [28, 29], denoted as *Color Glass Condensate*, or CGC, offers an alternative description of the nucleon in the small  $x$  regime, based on the qualitative argument that the spacial extension of the small  $x$  gluon's wave functions are large and can overlap across nucleons inside the nucleus, resulting in a reduction (or saturation) of the number of such gluons and the possibility for the incoming parton to interact coherently with several gluons of the target nucleus to form a  $c\bar{c}$  state. This approach describes PHENIX forward rapidity data better, but miss the mid-rapidity values and makes no prediction at negative rapidity. In fact, the rapidity range to which this approach is applicable at RHIC energies is still debated.

## 10 $J/\psi$ Production in Au + Au Collisions

The  $J/\psi$  nuclear modification factor  $R_{AA}$  has been measured in  $\sqrt{s_{NN}} = 200$  GeV Au + Au collisions by the PHENIX experiment. The latest results, obtained with the 2004 data set for the mid-rapidity points, and with the 2007 data set for the forward rapidity points, are shown in figure 9 [13].

The main features of these measurements are:

- a significant suppression of the  $J/\psi$  yields with respect to scaled expectations from  $p + p$  collisions is observed for most central collisions at both mid and forward rapidity;
- the suppression is larger at forward rapidity than at mid rapidity, which is contrary to the behavior expected for any suppression mechanism that is based on the local energy density of the medium created during the collisions (the latter being larger at mid rapidity than at forward rapidity);
- the suppression is smaller than what would have been naively expected by extrapolating measurements performed on the SPS at CERN, based on energy density arguments;

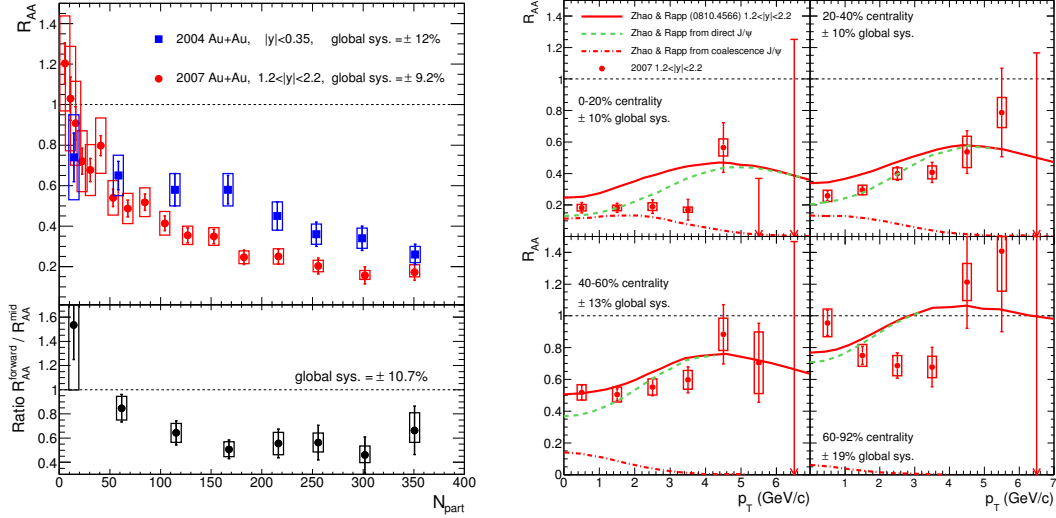


Figure 9:  $J/\psi$  nuclear modification factor  $R_{AA}$  in  $\sqrt{s_{NN}} = 200$  GeV Au + Au collisions; left: as a function of  $N_{part}$  the number of nucleons participating to a Au + Au collision at a given centrality; right: as a function of the  $J/\psi$  transverse momentum in four centrality bins.

- within large uncertainties, there is no dependence of the nuclear modification factor on the  $J/\psi$  transverse momentum.

Note that similar measurements have been performed in Cu + Cu collisions at the same energy. The values measured for  $R_{AA}$  in these conditions match the one obtained in Au + Au for a similar value of  $N_{part}$ , the number of nucleons participating to a collision at a given centrality.

These measurements have been compared to an extensive set of calculations that include one or several of the following ingredients [13]:

- modifications of the parton distribution functions;
- breakup of the  $J/\psi$  or of its pre-resonant  $c\bar{c}$  state;
- suppression of the  $J/\psi$  production yields in the context of the Color Glass Condensate;
- contribution from B meson decays;
- suppression of the prompt  $J/\psi$  via color screening in a quark gluon plasma;
- statistical or kinetic formation of  $J/\psi$  in a QGP by the coalescence uncorrelated charm quarks;

The first three effects above are so-called *cold nuclear matter* effects, and do not necessitate the formation of a QGP (note that the description of the collision in terms of a CGC and in terms of modified parton distribution functions plus break-up cross section are mutually exclusive). These effects alone are unable to reproduce the suppression observed in Au + Au central collisions. They are, however, capable of describing at least part of the difference observed between the mid and forward rapidity results.

The last two effects both require the presence of a quark gluon plasma, and impact the  $J/\psi$  production yields in opposite directions. Calculations that include these two competing effects together with cold nuclear matter effects are able to reproduce, at least qualitatively, the measured  $R_{AA}$  values both as a function of the collision centrality and the  $J/\psi$  transverse momentum [30]. In such calculations, the impact of the  $J/\psi$  formation by the coalescence of uncorrelated charm quarks is limited and only affects low  $p_T$   $J/\psi$ s.

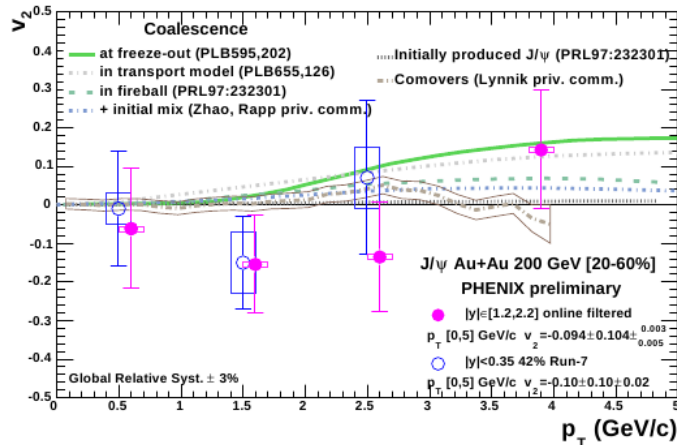


Figure 10:  $J/\psi$ 's production azimuthal anisotropy parameter  $v_2$  as a function of the  $J/\psi$   $p_T$  in semi-central  $\sqrt{s_{NN}} = 200$  GeV Au + Au collisions, and comparison to models.

In an attempt to single out the possible formation of  $J/\psi$  by the coalescence of uncorrelated charm quarks, PHENIX has also measured the  $J/\psi$ 's production azimuthal anisotropy with respect to the collision's reaction plane (formed by the beam axis and the vector that joins the center of the two colliding nuclei), in A + A collisions, as a function of the  $J/\psi$   $p_T$ . This anisotropy, characterized by the  $v_2$  parameter, the second coefficient of the Fourier transform of the  $J/\psi$ 's azimuthal distribution, is expected to be small but non-zero for such  $J/\psi$ s, as a consequence of the measured non-zero azimuthal anisotropy for  $D$  mesons. The obtained results, presented in figure 10 have large uncertainties due to the limited statistics available for the measurement. They show no significant deviation from zero and are not able to discriminate between models that do or do not include charm quark coalescence. A zero value for the  $J/\psi$ 's  $v_2$  parameter has later on be confirmed by more precise measurements performed by the STAR collaboration, and validated by theoretical calculations: since the charm quark coalescence mechanism would only create low  $p_T$   $J/\psi$ , whereas a non-zero  $J/\psi$   $v_2$  could only be visible for high enough  $p_T$ , where *prompt*  $J/\psi$  dominate, no significant  $J/\psi$   $v_2$  is in fact expected at RHIC energies.

## 11 Conclusion and Perspectives

The production of the  $J/\psi$  meson has been extensively studied at RHIC, in  $p + p$ ,  $d + A$  and A + A collisions to quantify the effects of the surrounding cold and hot nuclear matter created during heavy ion collisions. The SPHN group has played a crucial role at all steps of these studies over the past 7 years, by contributing to the maintenance of the muon detector at forward rapidity, taking the responsibility of the reconstruction software of the forward rapidity data and of the simulation software at both mid- and forward rapidities, and by actively participating to almost all the  $J/\psi$  related analysis performed in PHENIX during this period.

The partial conclusions of these studies are that:

- $J/\psi$  measurements in  $p + p$  collisions have become precise enough to discriminate between some  $J/\psi$  production mechanism models and parton distribution functions, although some crucial measurements are still missing, such as a precise measurement of the  $J/\psi$  polarization or the measurement of feed-down contributions from higher mass resonances and B mesons. (Some of these measurements are becoming available but with limited statistics);
- a number of effects can significantly modify the production of  $J/\psi$  in heavy ion collisions in absence of a quark gluon plasma. These cold nuclear matter effects are still largely unconstrained and existing

calculations are not capable of simultaneously reproducing all the available measurements;

- a significant suppression of the  $J/\psi$  meson is observed in Au + Au (and Cu + Cu) central collisions, that extends beyond the suppression inferred from cold nuclear matter effects only, and can therefore be attributed to the formation of a hot dense medium during the collision, identified to a Quark Gluon Plasma, whose properties are still being studied. The suppression measured at RHIC can be more or less reproduced by calculations that include a large number of both cold and hot nuclear matter effects that sometime partially compensate. More measurements are required to nail down the relative contributions of these effects.

Since 2010,  $p + p$  and heavy ion (Pb + Pb) collisions are also recorded at the LHC at significantly larger center of mass energies per nucleon-nucleon collision ( $\sqrt{s_{NN}} = 2.76$  and 7 TeV). The ALICE experiment [7] is capable of measuring the production of heavy quarkonia resonances ( $J/\psi$  and  $\Upsilon$ , notably) in such collisions, which should help sorting out some of the issues raised above. It is notably equipped with one muon spectrometer capable of measuring the production of these resonances at forward rapidity ( $2.5 < y < 4$ ). The design of this spectrometer somewhat differs from the PHENIX muon detectors and allows to circumvent some of the shortcoming of the latter. A dipole magnet is used to bend the particle's trajectory in order to measure their momentum, in a way that makes the track reconstruction more straightforward than with the PHENIX radial magnetic field. Notably the particles trajectory in the detection planes that are located outside of this magnet can be considered as straight lines, in first approximation. Additionally, the detectors used for the tracking are two-dimensional multi-wire pad chambers, which significantly reduces the occupancy of the detector and the amount of overlapping clusters in central Pb + Pb collisions. As a consequence, no significant deterioration of the tracking capabilities have been observed between central and peripheral collisions so far. This is in strong contrast to the results shown in figure 3 for the PHENIX muon spectrometers.

The inclusive  $J/\psi$  production cross section have already been measured by Alice (and by the other three LHC experiments) in  $p + p$  collisions at both energies (2.76 and 7 TeV [31]). In Pb + Pb collisions, the  $J/\psi$  nuclear modification factor  $R_{AA}$  has also been measured in several bins of centrality at an energy  $\sqrt{s_{NN}} = 2.76$  TeV [32]. Although a significant suppression is observed, it is less pronounced than the one measured at RHIC, indicating that  $J/\psi$  formation by the coalescence of uncorrelated charm quarks might play a more important role at this energy. It is however too early to draw any firm conclusion from this observation and one should notably first quantify the amount of cold nuclear matter effects at the LHC (a first  $p + Pb$  run is expected to happen in Fall 2012). Also, first measurements of the production of the  $\Upsilon$  resonances are becoming available in both  $p + p$  and Pb + Pb collisions. More results should follow in the near future, using data collected during the LHC Fall 2011 Pb + Pb run.

## References

- [1] K. Adcox et al. PHENIX detector overview. *Nucl.Instrum.Meth.*, A499:469–479, 2003.
- [2] T. Matsui and H. Satz.  $J/\psi$  Suppression by Quark-Gluon Plasma Formation. *Phys. Lett.*, B178:416, 1986.
- [3] Carlos Lourenco, Ramona Vogt, and Hermine K. Woehri. Energy dependence of  $J/\psi$  absorption in proton-nucleus collisions. *JHEP*, 02:014, 2009. and references therein.
- [4] Benjamin Svetitsky. Diffusion of charmed quarks in the quark-gluon plasma. *Phys. Rev. D*, 37:2484–2491, May 1988.
- [5] A. Andronic, P. Braun-Munzinger, K. Redlich, and J. Stachel. Statistical hadronization of charm in heavy-ion collisions at SPS, RHIC and LHC. *Phys. Lett.*, B571:36–44, 2003.
- [6] R. L Thews and M. L Mangano. Momentum spectra of charmonium produced in a quark-gluon plasma. *Phys. Rev. C*, 73:014904, May 2006.

- [7] The ALICE Collaboration. The alice experiment at the cern lhc. *Journal of Instrumentation*, 3(08):S08002, 2008.
- [8] A. Adare et al. J/psi production vs centrality, transverse momentum, and rapidity in Au + Au collisions at  $\sqrt{s}(NN)^{1/2} = 200$ - GeV. *Phys. Rev. Lett.*, 98:232301, 2007.
- [9] A. Adare et al. J / psi production versus transverse momentum and rapidity in p+p collisions at  $\sqrt{s}(1/2) = 200$ -GeV. *Phys. Rev. Lett.*, 98:232002, 2007.
- [10] A. Adare et al. J/psi Production in sqrt (sNN)= 200 GeV Cu+Cu Collisions. *Phys. Rev. Lett.*, 101:122301, 2008.
- [11] A. Adare et al. Cold Nuclear Matter Effects on J/Psi as Constrained by Deuteron-Gold Measurements at sqrt(sNN) = 200 GeV. *Phys. Rev.*, C77:024912, 2008.
- [12] A. Adare et al. Cold Nuclear Matter Effects on J/psi Yields as a Function of Rapidity and Nuclear Geometry in Deuteron-Gold Collisions at sqrt(sNN) = 200 GeV. *Phys. Rev. Lett.*, 107:142301, 2011.
- [13] A. Adare et al. J/psi suppression at forward rapidity in Au+Au collisions at sqrt(sNN)=200 GeV. 2011.
- [14] R. Frühwirth. Application of Kalman filtering to track and vertex fitting. *Nuclear Instruments and Methods in Physics Research A*, 262:444–450, December 1987.
- [15] Volker Blobel and Claus Kleinwort. A new method for the high-precision alignment of track detectors. 2002.
- [16] Torbjörn Sjöstrand, Stephen Mrenna, and Peter Skands. A brief introduction to pythia 8.1. *Computer Physics Communications*, 178(11):852–867, 2008.
- [17] G. Corcella et al. HERWIG 6.5: an event generator for Hadron Emission Reactions With Interfering Gluons (including supersymmetric processes). *JHEP*, 01:010, 2001.
- [18] Miklos Gyulassy and Xin-Nian Wang. HIJING 1.0: A Monte Carlo program for parton and particle production in high-energy hadronic and nuclear collisions. *Comput. Phys. Commun.*, 83:307, 1994.
- [19] R. Brun et al. *CERN Program Library Long Write-up W5013*, 1994.
- [20] A. Adare et al. Ground and excited charmonium state production in p+p collisions at sqrt(s)=200 GeV. 2011.
- [21] Harald Fritzsch. Producing heavy quark flavors in hadronic collisions: A test of quantum chromodynamics. *Phys. Lett. B*, 67:217, 1977.
- [22] J. F. Amundson, Oscar J. P. Eboli, E. M. Gregores, and F. Halzen. Quantitative tests of color evaporation: Charmonium production. *Phys. Lett. B*, 390:323–328, 1997.
- [23] R. Baier and R. Ruckl. Hadronic Production of J/psi and Upsilon: Transverse Momentum Distributions. *Phys. Lett. B*, 102:364, 1981.
- [24] Geoffrey T. Bodwin, Eric Braaten, and G. Peter Lepage. Rigorous QCD analysis of inclusive annihilation and production of heavy quarkonium. *Phys. Rev.*, D51:1125–1171, 1995.
- [25] Michael L. Miller, Klaus Reygers, Stephen J. Sanders, and Peter Steinberg. Glauber modeling in high energy nuclear collisions. *Ann. Rev. Nucl. Part. Sci.*, 57:205–243, 2007.
- [26] R. Vogt. Shadowing and absorption effects on J/psi production in d A collisions. *Phys. Rev.*, C71:054902, 2005.
- [27] K. J. Eskola, H. Paukkunen, and C. A. Salgado. EPS09 - a New Generation of NLO and LO Nuclear Parton Distribution Functions. *JHEP*, 04:065, 2009.

- [28] D. Kharzeev and K. Tuchin. Open charm production in heavy ion collisions and the color glass condensate. *Nucl. Phys.*, A735:248–266, 2004.
- [29] Dmitri Kharzeev and Kirill Tuchin. Signatures of the color glass condensate in J/psi production off nuclear targets. *Nucl. Phys.*, A770:40–56, 2006.
- [30] Xingbo Zhao and Ralf Rapp. Charmonium in medium: From correlators to experiment. *Phys. Rev. C*, 82:064905, Dec 2010.
- [31] K. Aamodt et al. Rapidity and transverse momentum dependence of inclusive J/psi production in pp collisions at  $\sqrt{s} = 7$  TeV. *Phys. Lett.*, B704:442–455, 2011.
- [32] Hugo Pereira Da Costa. J/psi production in pp and Pb-Pb with ALICE at the LHC. 2011.